

Small-Molecule Acceptor Based on the Heptacyclic Benzodi(cyclopentadithiophene) Unit for Highly Efficient Nonfullerene Organic Solar Cells

Bin Kan,^{†,‡} Huanran Feng,^{†,‡} Xiangjian Wan,^{†,‡} Feng Liu,^{||} Xin Ke,^{†,‡} Yanbo Wang,^{†,‡} Yunchuang Wang,^{†,‡} Hongtao Zhang,^{†,‡} Chenxi Li,^{†,‡} Jianhui Hou,^{§,¶} and Yongsheng Chen^{*,†,‡,¶}

[†]The Key Laboratory of Functional Polymer Materials and State Key Laboratory and Institute of Elemento-Organic Chemistry, Collaborative Innovation Center of Chemical Science and Engineering (Tianjin), College of Chemistry, Nankai University, Tianjin 300071, China

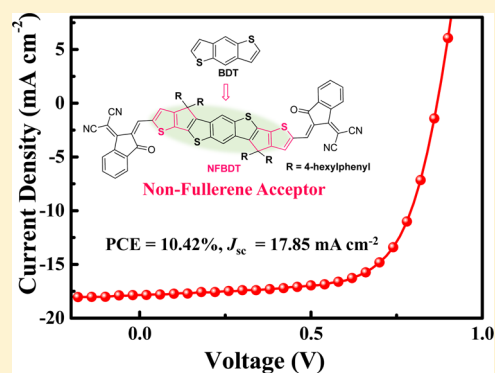
[‡]School of Materials Science and Engineering, The National Institute for Advanced Materials, Nankai University, Tianjin 300071, China

[§]State Key Laboratory of Polymer Physics and Chemistry, Beijing National Laboratory for Molecular Sciences, Institute of Chemistry, Chinese Academy of Sciences, Beijing 100190, China

^{||}Department of Physics and Astronomy, Shanghai Jiaotong University, Shanghai 200240, China

Supporting Information

ABSTRACT: A new nonfullerene small molecule with acceptor–donor–acceptor (A–D–A) structure, namely, NFBDT, based on a heptacyclic benzodi(cyclopentadithiophene) (FBDT) unit using benzo[1,2-*b*:4,5-*b'*]-dithiophene as the core unit, was designed and synthesized. Its absorption ability, energy levels, thermal stability, as well as photovoltaic performances were fully investigated. NFBDT exhibits a low optical bandgap of 1.56 eV resulting in wide and efficient absorption that covered the range from 600 to 800 nm, and suitable energy levels as an electron acceptor. With the widely used and successful wide bandgap polymer PBDB-T selected as the electron donor material, an optimized PCE of 10.42% was obtained for the PBDB-T:NFBDT-based device with an outstanding short-circuit current density of 17.85 mA cm⁻² under AM 1.5G irradiation (100 mW cm⁻²), which is so far among the highest performance of NF-OSC devices. These results demonstrate that the BDT unit could also be applied for designing NF-acceptors, and the fused-ring benzodi(cyclopentadithiophene) unit is a prospective block for designing new NF-acceptors with excellent performance.



INTRODUCTION

Solution-processed organic solar cells (OSCs) with bulk heterojunction (BHJ) architecture have drawn increasing attention because of their unique advantages such as light weight and flexibility.^{1,2} Due to the evolution of novel donor materials, including polymers and small molecules, and device optimization, power conversion efficiencies (PCEs) better than 10% have been obtained for fullerene-based OSCs recently.^{3–9}

The great success of the fullerene derivative acceptors (e.g., PCBM, ICBA) could be ascribed to some of their fundamental properties, including high electron affinity and electron mobility, and ability to form appropriate phase separation.^{10–12}

Despite these encouraging results of fullerene-based OSCs, the fullerene derivatives possess some intrinsic drawbacks, for example, weak absorption ability in the visible region, high cost in their preparation and purification processes, and weak chemical and electronic adjustability. To overcome these issues, nonfullerene (NF) small-molecule acceptors with wide and

efficient absorption, facile synthesis, and more finely tuned energy levels have developed rapidly in past few years.^{13–15}

Numerous NF small-molecule acceptors have been reported on the basis of a variety of π -conjugated moieties, such as perylene diimide (PDI), naphthalene diimide (NDI), fluo-ranthenene-fused diimide, diketopyrrolopyrrole (DPP), etc.^{16–21} To date, the performances of some NF-based OSCs exceed those of their fullerene-based control devices.^{22–26} Among these, small-molecule acceptors with the acceptor–donor–acceptor (A–D–A) backbone architecture, similar as the widely used and rather successful small-molecule donors,²⁷ have drawn particular interest due to their easily tuned energy levels and high device performances.^{28–32} As a typical and successful case, Zhan et al. reported a series of A–D–A-type NF-acceptors (such as ITIC, ITIC-Th, and IDIC) using

Received: February 2, 2017

Published: March 16, 2017

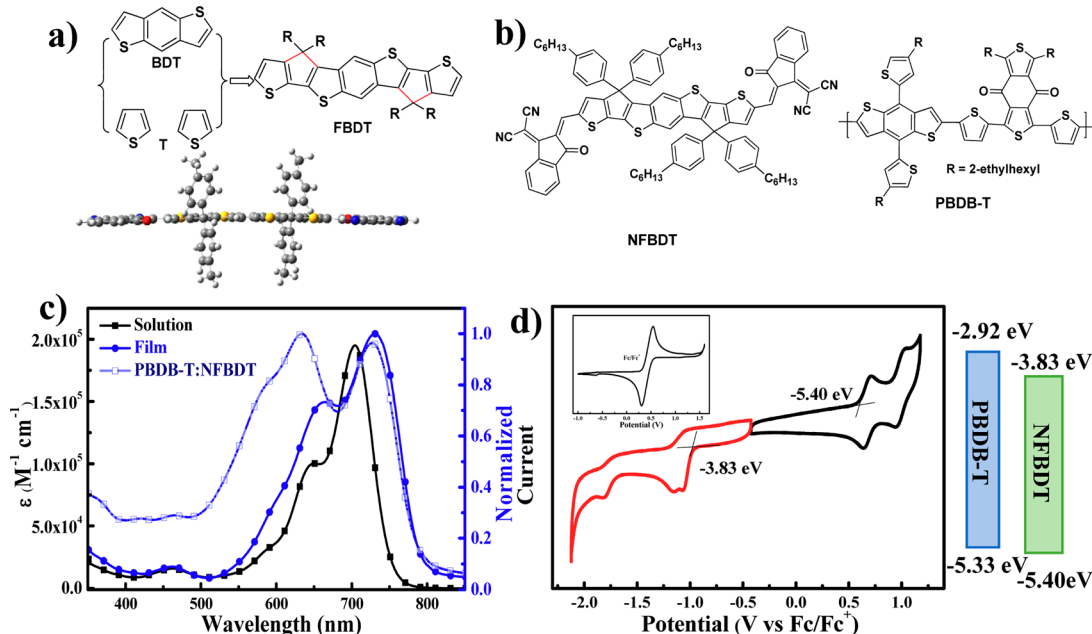
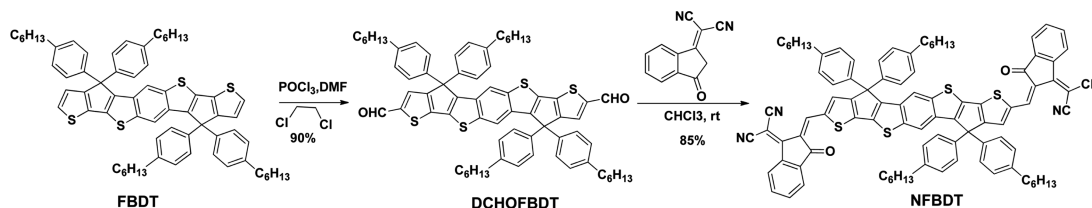


Figure 1. Chemical structure of the (a) FBDT unit, and (b) NFBDT acceptor and PBDB-T donor. (c) Absorption spectra of NFBDT in chloroform solution and thin film, and the absorption of PBDB-T:NFBDT blend film. (d) Cyclic voltammogram of NFBDT in dichloromethane solution with 0.1 M Bu_4PF_6 as the supporting electrolyte with a scan speed of 100 mV s^{-1} and the energy diagrams of PBDB-T and NFBDT; the inset shows the CV curve of the internal reference (Fc/Fc^+).

Scheme 1. Synthetic Scheme of NFBDT



extended fused-ring indacenodithieno[3,2-*b*]thiophene (IDTT) or indacenothiophene (IDT) as a central building block.^{33–36} With a careful choice of donor materials and systematic device optimization, PCEs over 10% have been obtained for devices based on ITIC and its analogs.^{24,37–39}

Recently, we have reported a NF-acceptor FDICTF based on a ladder-type core unit by fusing the fluorene with the adjacent thiophene units.⁴⁰ In contrast to its unfused counterpart molecule DICTF,⁴¹ FDICTF showed red-shifted absorptions, and higher and balanced charge mobilities after blending with the donor materials. Due to the enhanced short-circuit current (J_{sc}), a PCE over 10% has been achieved for FDICTF-based devices. Currently, improving J_{sc} is probably one of the most pursued strategies for further enhancement of the overall OSC performance in the community. For the A–D–A-type NF molecules, planar fused central units with a delocalized π -electron cloud could give bathochromically shifted absorptions, which are beneficial for harvesting photons and enhancing J_{sc} . Thus, developing new ladder-type fused units as the central building blocks utilizing the A–D–A architecture appears to be a good way to search higher performance NF-acceptors.

Benzo[1,2-*b*:4,5-*b'*]dithiophene (BDT) is a rather widely used building block in the OSC community, partially due to its symmetric and planar conjugated structure.^{42–44} Numerous polymer/small-molecule donor materials employing the BDT unit have been developed,^{45–47} and some, such as PTB7-Th,

DR3TSBTD, have shown excellent device performances.^{48,49} Here, with the strategy rather successfully used for the electron donor molecules, we have reported a new NF small-molecule with A–D–A architecture, namely, NFBDT (Figure 1b), with a heptacyclic benzodi(cyclopentadithiophene) (FBDT) unit based on BDT as the central unit and 2-(2,3-dihydro-3-oxo-1*H*-inden-1-ylidene)propanedinitrile (INCN) as ending group. In the FBDT unit, the BDT core units are covalently rigidified at its 3,7-positions with two external fused thiophene (T) units by the sp^3 -carbon bridges (Figure 1a). This design is expected to ensure the target molecule NFBDT to not only have a planar backbone but also avoid strong aggregation in the solid state, required for the delicate balance of many and complex factors for high performance such as high absorption, mobility, and ideal morphologies in the BHJ layer. Indeed, NFBDT exhibits a low optical bandgap ($E_{\text{g}}^{\text{opt}}$) of 1.56 eV resulting in wide and efficient absorption that covered the range 600–800 nm, and suitable energy levels as an electron acceptor (discussed below). On the basis of these parameters, a widely used and rather successful wide bandgap polymer, poly[(2,6-(4,8-bis(5-(2-ethylhexyl)thiophen-2-yl)-benzo[1,2-*b*:4,5-*b'*]dithiophene)-*alt*-(5,5-(1',3'-di-2-thienyl-5',7'-bis(2-ethylhexyl)benzo[1',2'-*c*:4',5'-*c'*]dithiophene-4,8-dione))] (known as PBDB-T, as shown in Figure 1b), was selected as the donor material. The combination of PBDB-T and NFBDT offered an excellent complementary absorption range from 500 to 800 nm (Figure

Table 1. Optical and Electrochemical Data of NFBDT

compd	$\lambda_{\max}^{\text{sol}}$ (nm)	$\lambda_{\max}^{\text{film}}$ (nm)	$\lambda_{\text{edge}}^{\text{film}}$ (nm)	$E_{\text{g}}^{\text{opt}}$ (eV)	HOMO (eV)	LUMO (eV)	E_{g}^{cv} (eV)
NFBDT	703	731	795	1.56	-5.40	-3.83	1.57

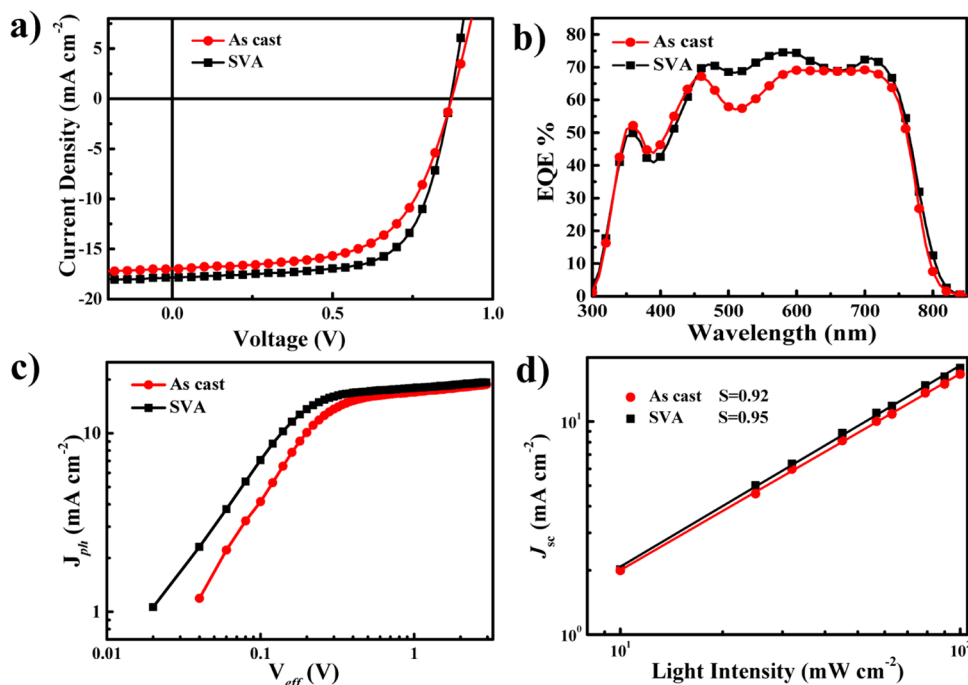


Figure 2. (a) Current density–voltage (J – V) curves of the devices based on PBDB-T:NFBDT without and with SVA under the illumination of AM 1.5G (100 mW cm⁻²). (b) EQE spectra of the as-cast device and SVA-treated device. (c) J_{ph} versus V_{eff} and (d) light-intensity (P) dependence of J_{sc} of the corresponding devices.

1c). There is an initial PCE of 8.99% for the PBDB-T:NFBDT-based devices with a high J_{sc} near 17 mA cm⁻² without any post-treatment. After the solvent vapor annealing treatment, the performance was enhanced to 10.42% (with a V_{oc} of 0.868 V, an outstanding J_{sc} of 17.85 mA cm⁻², and fill factor (FF) of 67.2%), which is so far among the best performance for NF-OSC devices. These results indicate that this novel acceptor, as one of the very few NF-acceptors offering >10% PCEs, might work as another platform with various small molecules and polymer donor materials to achieve high performance OSCs.

RESULTS AND DISCUSSION

Synthesis and Thermal Properties. The synthetic route of NFBDT is shown as Scheme 1, and their detailed synthetic procedures and characterization data can be found in the Supporting Information (SI). The central unit FBDT was synthesized according to the literature method (Scheme S1).⁵⁰ The dialdehyde compound DCHOFBDT was prepared by the Vilsmeier–Haack reaction as a white-yellow solid. The desired product NFBDT was then obtained by the Knoevenagel condensation of the dialdehyde compound with INCN in a high yield. The chemical structure of NFBDT was characterized and confirmed by NMR data, mass spectra, and elemental analysis detailed in the Experimental Section in the SI. This molecule exhibits high solubility in common organic solvents (e.g., chloroform and chlorobenzene) and excellent thermal stability up to 360 °C under nitrogen atmosphere as measured by thermogravimetric analysis (TGA, Figure S1a). From the differential scanning calorimetry (DSC) curve (Figure S1b), no

obvious melting point or recrystallization point was observed, indicating its weak crystallinity.

The molecular structure of NFBDT was investigated by using density functional theory (DFT) at the B3LYP/6-31G* level, and its optimized geometry is shown in Figure 1a. It can be seen that the conjugation backbone of NFBDT is highly planar mainly due to the excellent planarity of the core fused-ring unit, which is supported by the observed π – π stacking as evidenced by two-dimensional grazing-incidence X-ray diffraction (2D-GIXD) (Figure 4). Furthermore, the other four 4-hexylphenyl units exhibit a $\sim 110^\circ$ dihedral angle to its planar backbone, and thus can avoid severe self-aggregation and large-scale phase separation in the blend films for optimal morphology in the active layer.

Photophysical and Electrochemical Properties. The absorption spectra of NFBDT in solution and as a thin film are presented in Figure 1c. NFBDT in dilute chloroform solution shows an absorption peak at 703 nm with a high maximum extinction coefficient of 1.9×10^5 M⁻¹ cm⁻¹. In comparison with the solution absorption, a NFBDT film displays an obviously red-shifted absorption peak located at 731 nm, indicative of some ordered structure and π – π stacking interactions in the film due to its coplanar backbone. The absorption onset of NFBDT is located at ~ 795 nm, which corresponds to a low $E_{\text{g}}^{\text{opt}}$ of 1.56 eV. As shown in Figure 1c, the combination of PBDB-T and NFBDT provides a rather complementary absorption which covered almost the entire visible sunlight range from 500 to 800 nm, which is critical to achieve high photocurrent.

Table 2. Device Parameters of OSCs Based on PBDB-T:NFBBDT without and with SVA, Measured under the Illumination of AM 1.5G (100 mW cm^{-2})

treatment	V_{oc} (V)	J_{sc} (mA cm^{-2})	FF%	PCE%	PCE _{ave} %	R_s ($\Omega \text{ cm}^2$)	R_{sh} ($\Omega \text{ cm}^2$)
as-cast	0.872	16.97	60.8	8.99	8.80 ± 0.14	9.0	923.6
SVA	0.868	17.85	67.2	10.42	10.15 ± 0.17	6.0	1980.2

Cyclic voltammetry (CV) was used to investigate the energy level of NFBBDT in dichloromethane solution as presented in Figure 1d. Electrochemical and optical data are summarized in Table 1. The energy levels of the highest occupied molecular orbital (HOMO) estimated from the onset oxidation and lowest unoccupied molecular orbital (LUMO) calculated from the reduction potential are -5.40 and -3.83 eV, respectively. As shown in Figure 1d, the LUMO energy offset between NFBBDT and PBDB-T (-2.92 eV) is 0.91 eV, which is large enough for efficient electron transfer from PBDB-T to NFBBDT.³⁹ Although the HOMO energy offset for the PBDB-T:NFBBDT system is merely 0.07 eV (data obtained from CV of their solutions, see Figure 1d and Figure S2), the hole transfer from the NFBBDT acceptor to PBDB-T donor seems also to be highly efficient, confirmed by its reasonably high external quantum efficiency (EQE) values of the optimal device in the range from 650 to 780 nm and the photoluminescence (PL) quenching measurement as discussed below.

Photovoltaic Properties. To evaluate the potential of NFBBDT in OSCs as an electron acceptor, solution-processed devices were fabricated using PBDB-T as electron donor with the device structure of ITO/PEDOT:PSS (poly(3,4-ethylenedioxythiophene):poly(styrenesulfonate))/PBDB-T:NFBBDT/PDIN (*N,N'*-bis(propylenedimethylamine)-3,4:9,10-perylene diimide)/Al, where PDIN is an efficient cathode interlayer developed by Li et al. (shown as Figure S3).⁵¹ After device optimization (Tables S1–S5), the best donor/acceptor weight ratio was 1:0.8, and the thickness of the active layer was ~ 100 nm. OSC devices based on the as-cast PBDB-T:NFBBDT film gave a promising PCE of 8.99% with an open-circuit voltage (V_{oc}) of 0.872 V, a high J_{sc} of 16.97 mA cm^{-2} , and an FF of 60.8% . After SVA treatment, the PCE increased to 10.42% with a V_{oc} of 0.868 V, a remarkable J_{sc} of 17.85 mA cm^{-2} and an FF of 67.2% . To the best of our knowledge, this efficiency is among the top performance for current solution-processed NF-OSCs. The stability of the optimized device under continuous heating at 100 °C was investigated as shown in Figure S4. After heating for 1.5 h, the PCE decreases $\sim 14\%$ and then remains almost stable. The current density–voltage (J – V) curves of the as-cast and SVA-treated devices were shown as Figure 2a, and their corresponding photovoltaic parameters are summarized in Table 2.

The EQE spectra of devices without and with SVA are presented as Figure 2b. Together with the absorption shown in Figure 1c, the high and broad EQEs over the entire range from 300 to 800 nm suggest that both polymer donor and NF-acceptor made a considerable and complementary contribution to the whole J_{sc} values. The EQE values for a device with SVA were much higher than those for the as-cast BHJ device, reaching a maximum value of 75% and over 70% across the range 530 – 720 nm, which are indicative of a highly efficient photoelectron conversion process in the SVA-treated device. Importantly, rather high EQE values in the range 650 – 750 nm, where the light absorption should be mainly ascribed to the

acceptor component NFBBDT, illustrate an efficient hole transfer process from NFBBDT-acceptor to polymer donor even with ~ 0.07 eV HOMO energy offset. To further confirm the charge transfer behavior in the optimized blend films, PL quenching experiments were carried out at the excitation wavelength of 550 and 670 nm. As shown in Figure S5, the quenching efficiencies for polymer donor and NF-acceptor are calculated to be 98% and 96% , respectively, supporting the above-mentioned results. The J_{sc} values calculated from the EQE curves are 16.4 and 17.6 mA cm^{-2} for the devices without and with SVA, respectively, which are within a reasonable mismatch to the J_{sc} values obtained from the corresponding J – V curves.

The plots of photocurrent (J_{ph}) versus the effective applied voltage (V_{eff}) for the devices without and with SVA were measured to comprehensively study the influence of SVA treatment on the excitation dissociation and charge collection properties in the devices (Figure 2c). $J_{ph} = J_L - J_D$, where J_L is the current density under illumination and J_D is the current density in the dark. $V_{eff} = V_o - V_a$, where V_a is the applied voltage and V_o is the voltage at which J_{ph} is zero.⁵² As can be seen from Figure 2c, when V_{eff} arrives at ~ 2 V, J_{ph} values for both devices reach saturation (J_{sat}), suggesting that charge recombination is minimized at higher voltage due to the high internal electric field in the devices. The charge dissociation and charge collection probability ($P(E, T)$) in the devices could be estimated by calculating the value of J_{ph}/J_{sat} .⁵³ Under their short-circuit and maximal power output conditions, $P(E, T)$ values are 92% , 71% for the as-cast device, and 94% , 81% for the device with SVA, respectively. The increased $P(E, T)$ values indicate that the SVA-treated device exhibits higher exciton dissociation and more efficient charge collection efficiency compared to those of the as-cast device.^{52,53} In addition, compared with the as-cast device, the device with SVA treatment exhibits a relatively lower series resistance (R_s) and a higher shunt resistance (R_{sh}), indicating a better ohmic contact in the device with SVA (Table 2) and thus leading to a higher FF.

To further probe the charge recombination behavior in the devices, the light-intensity (P) dependence of J_{sc} was then measured. The relationship between J_{sc} and P can be represented by the power-law equation $J_{sc} \propto P^\alpha$, whereas the power-law exponent α implies the extent of bimolecular recombination. As presented in Figure 2d, the α value for the device with SVA is 0.95 , which is higher than 0.92 for the as-cast device. This suggests that less bimolecular recombination occurred in the device with SVA, supporting its high J_{sc} and FF.⁵³

Morphology Characterization. The influence of SVA on the active layer morphologies was studied by atomic force microscopy (AFM) using the tapping mode. As can be seen in Figure S6, the blend films without and with SVA are uniform and smooth. No large phase separations were observed for both films, indicating good miscibility between PBDB-T and NFBBDT. The root-mean-square surface roughness values for as-cast and SVA-treated films are 1.44 and 1.41 nm,

respectively. From the TEM images (Figure 3), compared to those of the as-cast film, a more defined phase separation of

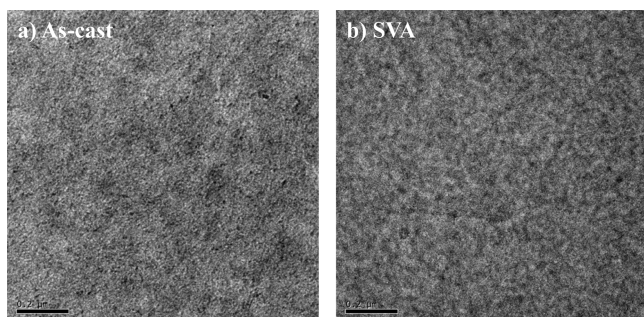


Figure 3. TEM images for (a) the as-cast blend film and (b) the SVA-treated blend film. The scale bars are 200 nm.

donor and acceptor with a bicontinuous interpenetrating network was observed in the film with SVA. This benefits exciton dissociation and charge transport, and thus results in high FFs.

The microstructures of NFBDT film and PBDB-T:NFBDT blend films were characterized using 2D-GIXD.⁵⁴ Out-of-plane and in-plane line cuts of GIXD for blend films are presented in Figure 4. As can be seen from Figure 4a, NFBDT exhibits an

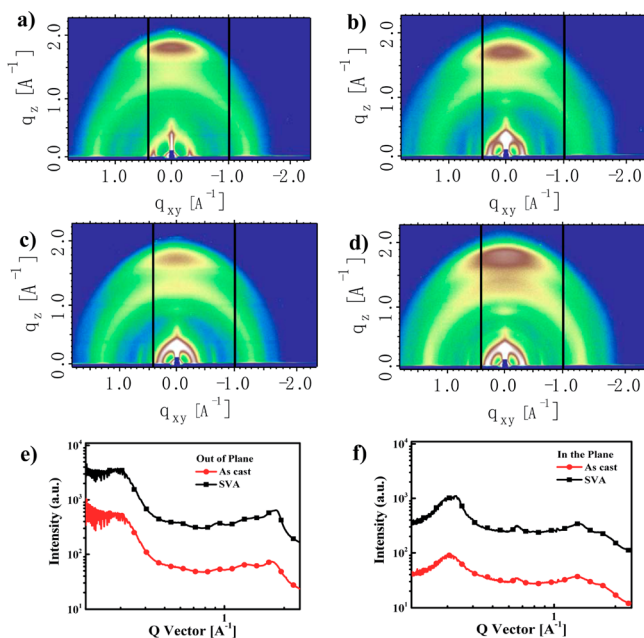


Figure 4. GIXD patterns for pure films of (a) NFBDT and (b) PBDB-T, and blend films (c) without treatment and (d) with SVA. (e) Out-of-plane and (f) in-plane line cuts of the GIXD patterns for the blend films.

obvious (010) diffraction peak in the out-of-plane (OOP) direction and a clear (100) diffraction peak along its in-plane (IP) direction, suggesting that NFBDT has a preferred face-on orientation relative to the substrate. Polymer PBDB-T also takes a preferential face-on orientation as seen from π - π stacking diffraction in the OOP direction (Figure 4b). In the blend films, the alkyl-alkyl and π - π stacking regions show combined diffraction features from PBDB-T and NFBDT, and appear as broad peaks that cannot be easily separated.

Combined (010) peaks in the OOP direction are observed in both blend films, which means NFBDT and PBDB-T still adopt a preferred face-on orientation in blend films. In addition, enhanced diffraction peak intensities in the SVA-treated blend film are indicative of improved molecule packing, which should be beneficial for charge transport.⁵⁵ By using the space-charge limited current (SCLC) method with the electron and hole only device (Figure S7), the charge transport properties of the PBDB-T:NFBDT films were investigated. The electron and hole mobilities for the as-cast film are calculated to be 0.81×10^{-4} and $2.19 \times 10^{-4} \text{ cm}^{-2} \text{ V}^{-1} \text{ s}^{-1}$, respectively. After SVA treatment, the electron and hole mobilities are improved to 1.38×10^{-4} and $3.68 \times 10^{-4} \text{ cm}^{-2} \text{ V}^{-1} \text{ s}^{-1}$, respectively. The enhanced mobilities lead to the higher FF and J_{sc} after SVA treatment.

CONCLUSION

In conclusion, a new acceptor-donor-acceptor (A-D-A) and ladder-type acceptor NFBDT using a BDT-based fused central unit was designed and synthesized. NFBDT exhibited a low E_g^{opt} of 1.56 eV and efficient absorption in the 600–800 nm region. In combination with a wide bandgap polymer donor PBDB-T, its optimized device delivered a promising PCE of 10.42% with a remarkable J_{sc} of 17.85 mA cm^{-2} due to the efficient photoelectron conversion process in the device. Note that this newly designed material is one of the very few electron acceptor materials offering >10% PCEs. Furthermore, for the PBDB-T:NFBDT, an efficient hole transfer from the acceptor NFBDT to the donor PBDB-T was observed even with a rather small 0.07 eV HOMO energy offset. This might offer an important indicator for designing new donor and acceptor materials with the goal to maximize both V_{oc} and J_{sc} simultaneously. All of these demonstrate that this modified BDT unit could also be applied for designing other high performance NF-acceptors, and the fused-ring benzodi-(cyclopentadithiophene) unit is a promising block for it. With consideration of the wide versatility of chemical structures and energy levels of various donor materials, it is believed that this newly designed NF-acceptor might work as another promising electron acceptor choice to screen for high performance OSCs with various electron donor materials already available in the community.

ASSOCIATED CONTENT

Supporting Information

The Supporting Information is available free of charge on the ACS Publications website at DOI: 10.1021/jacs.7b01170.

Detailed synthetic procedures and characterization data as well as experimental results (PDF)

AUTHOR INFORMATION

Corresponding Author

*yschen99@nankai.edu.cn

ORCID

Jianhui Hou: 0000-0002-2105-6922

Yongsheng Chen: 0000-0003-1448-8177

Notes

The authors declare no competing financial interest.

ACKNOWLEDGMENTS

The authors gratefully acknowledge the financial support from the Ministry of Science and Technology of China (MoST) (2014CB643502 and 2016YFA0200200), and NSFC (91433101, 51422304, 51373078, 91633301).

REFERENCES

- (1) Li, G.; Zhu, R.; Yang, Y. *Nat. Photonics* **2012**, *6*, 153.
- (2) Service, R. F. *Science* **2011**, *332*, 293.
- (3) Collins, S. D.; Ran, N. A.; Heiber, M. C.; Nguyen, T. Q. *Adv. Energy Mater.* **2017**, 1602242.
- (4) Fu, P.; Guo, X.; Zhang, B.; Chen, T.; Qin, W.; Ye, Y.; Hou, J.; Zhang, J.; Li, C. *J. Mater. Chem. A* **2016**, *4*, 16824.
- (5) Jin, Y.; Chen, Z.; Dong, S.; Zheng, N.; Ying, L.; Jiang, X. F.; Liu, F.; Huang, F.; Cao, Y. *Adv. Mater.* **2016**, *28*, 9811.
- (6) Liu, X.; Li, X.; Li, Y.; Song, C.; Zhu, L.; Zhang, W.; Wang, H. Q.; Fang, J. *Adv. Mater.* **2016**, *28*, 7405.
- (7) Nian, L.; Gao, K.; Liu, F.; Kan, Y.; Jiang, X.; Liu, L.; Xie, Z.; Peng, X.; Russell, T. P.; Ma, Y. *Adv. Mater.* **2016**, *28*, 8184.
- (8) Wan, Q.; Guo, X.; Wang, Z.; Li, W.; Guo, B.; Ma, W.; Zhang, M.; Li, Y. *Adv. Funct. Mater.* **2016**, *26*, 6635.
- (9) Vohra, V.; Kawashima, K.; Kakara, T.; Koganezawa, T.; Osaka, I.; Takimiya, K.; Murata, H. *Nat. Photonics* **2015**, *9*, 403.
- (10) Ostroverkhova, O. *Chem. Rev.* **2016**, *116*, 13279.
- (11) Lu, L.; Zheng, T.; Wu, Q.; Schneider, A. M.; Zhao, D.; Yu, L. *Chem. Rev.* **2015**, *115*, 12666.
- (12) Yu, G.; Gao, J.; Hummelen, J. C.; Wudl, F.; Heeger, A. J. *Science* **1995**, *270*, 1789.
- (13) McAfee, S. M.; Topple, J. M.; Hill, I. G.; Welch, G. C. *J. Mater. Chem. A* **2015**, *3*, 16393.
- (14) Lin, Y.; Zhan, X. *Adv. Energy Mater.* **2015**, *5*, 1501063.
- (15) Nielsen, C. B.; Holliday, S.; Chen, H. Y.; Cryer, S. J.; McCulloch, I. *Acc. Chem. Res.* **2015**, *48*, 2803.
- (16) Fernandez-Lazaro, F.; Zink-Lorrie, N.; Sastre-Santos, A. *J. Mater. Chem. A* **2016**, *4*, 9336.
- (17) Meng, D.; Fu, H.; Xiao, C.; Meng, X.; Winands, T.; Ma, W.; Wei, W.; Fan, B.; Huo, L.; Doltsinis, N. L.; et al. *J. Am. Chem. Soc.* **2016**, *138*, 10184.
- (18) Tang, A.; Zhan, C.; Yao, J.; Zhou, E. *Adv. Mater.* **2017**, *29*, 1600013.
- (19) Wu, Q.; Zhao, D.; Schneider, A. M.; Chen, W.; Yu, L. *J. Am. Chem. Soc.* **2016**, *138*, 7248.
- (20) Zhao, R.; Dou, C.; Xie, Z.; Liu, J.; Wang, L. *Angew. Chem.* **2016**, *128*, 5399.
- (21) Hwang, Y. J.; Li, H.; Courtright, B. A.; Subramanian, S.; Jenekhe, S. A. *Adv. Mater.* **2016**, *28*, 124.
- (22) Baran, D.; Ashraf, R. S.; Hanifi, D. A.; Abdelsamie, M.; Gasparini, N.; Rohr, J. A.; Holliday, S.; Wadsworth, A.; Lockett, S.; Neophytou, M.; Emmott, C. J. M.; Nelson, J.; Brabec, C. J.; Amassian, A.; Salleo, A.; Kirchartz, T.; Durrant, J. R.; McCulloch, I. *Nat. Mater.* **2017**, *16*, 363.
- (23) Liu, J.; Chen, S.; Qian, D.; Gautam, B.; Yang, G.; Zhao, J.; Bergqvist, J.; Zhang, F.; Ma, W.; Ade, H.; et al. *Nat. Energy* **2016**, *1*, 16089.
- (24) Yang, Y.; Zhang, Z.-G.; Bin, H.; Chen, S.; Gao, L.; Xue, L.; Yang, C.; Li, Y. *J. Am. Chem. Soc.* **2016**, *138*, 15011.
- (25) Li, S.; Ye, L.; Zhao, W.; Zhang, S.; Mukherjee, S.; Ade, H.; Hou, J. *Adv. Mater.* **2016**, *28*, 9423.
- (26) Zhao, W.; Zhang, S.; Hou, J. *Sci. China: Chem.* **2016**, *59*, 1574.
- (27) Chen, Y.; Wan, X.; Long, G. *Acc. Chem. Res.* **2013**, *46*, 2645.
- (28) Dai, S.; Zhao, F.; Zhang, Q.; Lau, T.-K.; Li, T.; Liu, K.; Ling, Q.; Wang, C.; Lu, X.; You, W.; Zhan, X. *J. Am. Chem. Soc.* **2017**, *139*, 1336.
- (29) Gupta, V.; Bagui, A.; Singh, S. P.; Suman. *Adv. Funct. Mater.* **2017**, *27*, 1603820.
- (30) Holliday, S.; Ashraf, R. S.; Wadsworth, A.; Baran, D.; Yousaf, S. A.; Nielsen, C. B.; Tan, C.-H.; Dimitrov, S. D.; Shang, Z.; Gasparini, N.; et al. *Nat. Commun.* **2016**, *7*, 11585.
- (31) Wang, K.; Firdaus, Y.; Babics, M.; Cruciani, F.; Saleem, Q.; El Labban, A.; Alamoudi, M. A.; Marszalek, T.; Pisula, W.; Laquai, F.; Beaujuge, P. M. *Chem. Mater.* **2016**, *28*, 2200.
- (32) Zhang, H.; Liu, Y.; Sun, Y.; Li, M.; Ni, W.; Zhang, Q.; Wan, X.; Chen, Y. *Sci. China: Chem.* **2017**, *60*, 366.
- (33) Lin, Y.; Wang, J.; Zhang, Z. G.; Bai, H.; Li, Y.; Zhu, D.; Zhan, X. *Adv. Mater.* **2015**, *27*, 1170.
- (34) Lin, Y.; Zhang, Z.-G.; Bai, H.; Wang, J.; Yao, Y.; Li, Y.; Zhu, D.; Zhan, X. *Energy Environ. Sci.* **2015**, *8*, 610.
- (35) Lin, Y.; Zhao, F.; He, Q.; Huo, L.; Wu, Y.; Parker, T. C.; Ma, W.; Sun, Y.; Wang, C.; Zhu, D.; Heeger, A. J.; Marder, S. R.; Zhan, X. *J. Am. Chem. Soc.* **2016**, *138*, 4955.
- (36) Lin, Y.; He, Q.; Zhao, F.; Huo, L.; Mai, J.; Lu, X.; Su, C.-J.; Li, T.; Wang, J.; Zhu, J.; Sun, Y.; Wang, C.; Zhan, X. *J. Am. Chem. Soc.* **2016**, *138*, 2973.
- (37) Bin, H.; Gao, L.; Zhang, Z.-G.; Yang, Y.; Zhang, Y.; Zhang, C.; Chen, S.; Xue, L.; Yang, C.; Xiao, M.; Li, Y. *Nat. Commun.* **2016**, *7*, 13651.
- (38) Lin, Y.; Zhao, F.; Wu, Y.; Chen, K.; Xia, Y.; Li, G.; Prasad, S. K.; Zhu, J.; Huo, L.; Bin, H.; Zhang, Z.; Guo, X.; Zhang, M.; Sun, Y.; Gao, F.; Wei, Z.; Ma, W.; Wang, C.; Hodgkiss, J.; Bo, Z.; Inganäs, O.; Li, Y.; Zhan, X. *Adv. Mater.* **2017**, *29*, 1604155.
- (39) Zhao, W.; Qian, D.; Zhang, S.; Li, S.; Inganäs, O.; Gao, F.; Hou, J. *Adv. Mater.* **2016**, *28*, 4734.
- (40) Qiu, N.; Zhang, H.; Wan, X.; Li, C.; Ke, X.; Feng, H.; Kan, B.; Zhang, H.; Zhang, Q.; Lu, Y.; Chen, Y. *Adv. Mater.* **2017**, *29*, 1604964.
- (41) Li, M.; Liu, Y.; Ni, W.; Liu, F.; Feng, H.; Zhang, Y.; Liu, T.; Zhang, H.; Wan, X.; Kan, B.; Zhang, Q.; Russell, T. P.; Chen, Y. *J. Mater. Chem. A* **2016**, *4*, 10409.
- (42) Xiao, S.; Zhang, Q.; You, W. *Adv. Mater.* **2016**, 1601391.
- (43) Yao, H.; Ye, L.; Zhang, H.; Li, S.; Zhang, S.; Hou, J. *Chem. Rev.* **2016**, *116*, 7397.
- (44) Liang, Y.; Yu, L. *Acc. Chem. Res.* **2010**, *43*, 1227.
- (45) Dou, L.; Liu, Y.; Hong, Z.; Li, G.; Yang, Y. *Chem. Rev.* **2015**, *115*, 12633.
- (46) Lu, L.; Zheng, T.; Wu, Q.; Schneider, A. M.; Zhao, D.; Yu, L. *Chem. Rev.* **2015**, *115*, 12666.
- (47) Li, M.; Ni, W.; Wan, X.; Zhang, Q.; Kan, B.; Chen, Y. *J. Mater. Chem. A* **2015**, *3*, 4765.
- (48) Liao, S. H.; Jhuo, H. J.; Cheng, Y. S.; Chen, S. A. *Adv. Mater.* **2013**, *25*, 4766.
- (49) Kan, B.; Zhang, Q.; Li, M.; Wan, X.; Ni, W.; Long, G.; Wang, Y.; Yang, X.; Feng, H.; Chen, Y. *J. Am. Chem. Soc.* **2014**, *136*, 15529.
- (50) Chen, Y.-L.; Chang, C.-Y.; Cheng, Y.-J.; Hsu, C.-S. *Chem. Mater.* **2012**, *24*, 3964.
- (51) Zhang, Z.-G.; Qi, B.; Jin, Z.; Chi, D.; Qi, Z.; Li, Y.; Wang, J. *Energy Environ. Sci.* **2014**, *7*, 1966.
- (52) Blom, P. W.; Mihailitchi, V. D.; Koster, L. J. A.; Markov, D. E. *Adv. Mater.* **2007**, *19*, 1551.
- (53) Proctor, C. M.; Kuik, M.; Nguyen, T.-Q. *Prog. Polym. Sci.* **2013**, *38*, 1941.
- (54) Rivnay, J.; Mannsfeld, S. C.; Miller, C. E.; Salleo, A.; Toney, M. F. *Chem. Rev.* **2012**, *112*, 5488.
- (55) Liu, F.; Gu, Y.; Shen, X.; Ferdous, S.; Wang, H.-W.; Russell, T. P. *Prog. Polym. Sci.* **2013**, *38*, 1990.